

## Hydralazine-Based Schiff Base Ligand and Its Ni(II), Cu(II), and Zn(II) Complexes: Synthesis, Antibacterial Activity, and Molecular Docking Studies

Ayşe Kazancı Dağ<sup>1,a,\*</sup>, Ugur Comlekcioglu<sup>2,b</sup><sup>1</sup> Department of Chemistry, Faculty of Science, Kahramanmaraş Sutcu Imam University, Kahramanmaraş, 46050, Türkiye.<sup>2</sup> Department of Biology, Faculty of Science, Kahramanmaraş Sutcu Imam University, Kahramanmaraş, 46050, Türkiye.

\*Corresponding author e-mail address: aysekazancidag@ksu.edu.tr

### Research Article

#### History

Received: 30.12.2025

Accepted: 23.03.2026

### ABSTRACT

Hydrazones are strong electron-donating ligands capable of coordinating through nitrogen donor atoms. Hydrazones and their transition metal complexes have been extensively investigated due to their wide-ranging applications in pharmaceuticals, analytical reagents, and agrochemicals. In this study, a new Schiff base ligand (HAG) was synthesized from 2-hydroxy-4-(prop-2-yn-1-yloxy)benzaldehyde and hydralazine. The antibacterial activities of the ligand and its Cu(II), Ni(II), and Zn(II) complexes were evaluated. The synthesized compounds were characterized by elemental analysis, IR, <sup>1</sup>H NMR, and UV-Vis spectroscopy. Analytical data confirmed the formation of 1:2 (M:L) complexes, where M represents Cu(II), Ni(II), or Zn(II) ions and L represents the deprotonated hydrazone ligand. IR spectral data revealed that HAG coordinates in a tridentate manner via phthalazine nitrogen, azomethine nitrogen, and phenolic oxygen atoms. Antimicrobial studies showed that [Zn(AG)<sub>2</sub>] exhibited the strongest activity against *Staphylococcus aureus*, with a MIC value of 250 µg/mL, while [Cu(AG)<sub>2</sub>] and [Ni(AG)<sub>2</sub>] showed MIC values of 1000 µg/mL against the same strain.

**Keywords:** Antibacterial activity, Hydralazine, Schiff base

This article is licensed under a Creative Commons Attribution-NonCommercial 4.0 International License (CC BY-NC 4.0)

<sup>a</sup>  0000-0002-9352-2160<sup>b</sup>  0000-0001-9093-4496

## 1. Introduction

The investigation of hydralazine-based compounds is gaining increasing importance today due to their effective biological activities and coordination abilities [1,2]. Phthalazine derivatives have recently attracted increased pharmacological research interest due to their diverse biological activities, which include anti-inflammatory [3,4], antimicrobial [5–8], anticonvulsant [9], and anticancer [10,11] effects. Among hydrazine derivatives, one of the most important compounds in practice is 1-hydrazinopentalazine (hydralazine), which is used as an effective therapeutic agent, particularly in its hydrochloride derivative form, for rapidly controlling blood pressure in hypertensive crises [12]. Due to its pronounced antihypertensive effect, the mechanism of action and metabolic behavior of hydralazine have been the subject of numerous studies. However, its chemical instability during dilution, storage, and administration significantly limits the compound's clinical use [13]. This instability is reported to originate from the molecule's reactive hydrazine group. Hydralazine-derived Schiff bases have been recognized in recent years as important ligands in coordination chemistry due to their strong chelating capacity and various biological activities [14,15].

It has been clearly demonstrated that hydrazone metal complexes have a wide range of potential applications in various fields, including medical applications, insecticides, and analytical reagents [16]. Furthermore, numerous studies have shown that these complexes exhibit important biological properties, including antitumor, anticancer, antimalarial, and antibacterial activities [17]. Newly synthesized hydrazone-derived metal complexes can exhibit different physicochemical properties and reactivity profiles compared to free ligands. This is related to the fact that the electron-donating/accepting character of the ligand, its structural properties, and its position within the coordination sphere directly affect the biological activities of the resulting complexes and can either increase or decrease these activities. Furthermore, such metal complexes are also widely used as model systems in the investigation of different chemical and biological processes [15,18].

Although several hydralazine-derived hydrazone metal complexes have been reported, most studies have focused primarily on structural characterization or general antimicrobial screening. Limited attention has been given to hydralazine-based Schiff bases bearing propargyl-functionalized aromatic aldehydes and their comparative

biological evaluation supported by molecular docking analysis. In this context, the present study introduces a structurally modified hydralazine-derived ligand containing a propargyl ether substituent and systematically evaluates the influence of different metal ions (Cu(II), Ni(II), Zn(II)) on antibacterial activity and protein-binding affinity.

In this study, we have prepared a new hydrazine based Schiff base ligand and its metal (Cu(II), Ni(II) and Zn(II))

complexes. Synthesized compounds were characterized by spectroscopic and analytic techniques. The compounds were screened for their antibacterials against *Escherichia coli* ATCC 35218, *Micrococcus luteus* ATCC 9341, and *Staphylococcus aureus* ATCC 25923. Finally, molecular dockings using sortase A (PDB ID: 1T2W), DNA gyrase (PDB ID: 3U2D), FtsA (PDB ID: 3WQU), and undecaprenyl diphosphate synthase (UPPS; PDB ID: 4H8E) were studied.

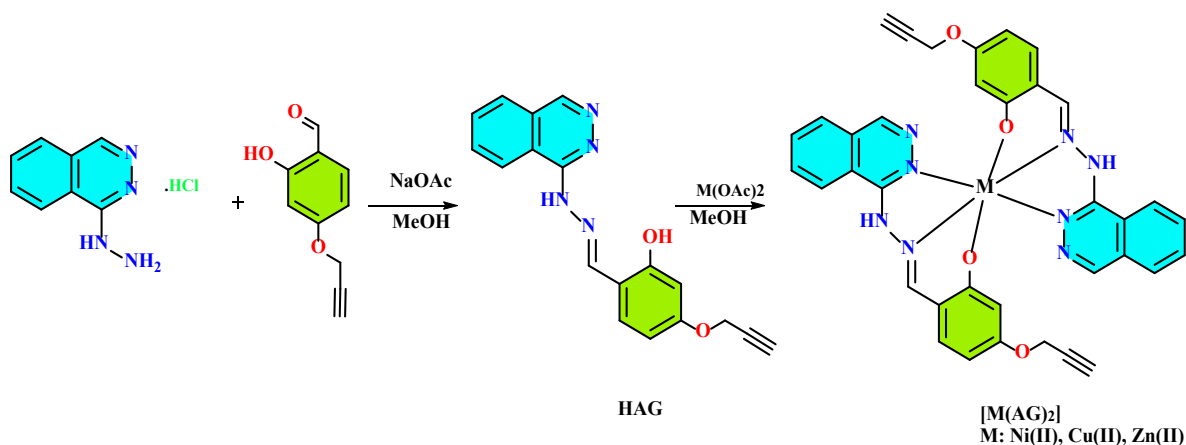


Figure 1. Synthesis of Schiff Base ligand and its Ni(II), Cu(II) and Zn(II) complexes.

## 2. Materials and Methods

### 2.1 Materials

All solvents and the starting materials including hydralazine hydrochloride salt, were purchased from Sigma Aldrich and used as received. 2-Hydroxy-4-(prop-2-yn-1-yloxy)benzaldehyde was synthesized according to the reported method [19,20]. FT-IR spectra were recorded on a Shimadzu IRTracer-100 spectrometer using the ATR method in the range 4000–450  $\text{cm}^{-1}$ .  $^1\text{H}$  and  $^{13}\text{C}$  NMR spectra were recorded on a 600 MHz spectrometer in DMSO- $d_6$  at 25 °C. UV-Vis spectra were measured in DMF ( $1.0 \times 10^{-5}$  M) using a UV-Vis spectrophotometer at room temperature.

### 2.2 Preparation of Hydrazone Ligand (HAG)

Hydralazine hydrochloride (0.01 mol) was dissolved in 20 mL of methanol under stirring at room temperature. Subsequently, 2-hydroxy-4-(prop-2-yn-1-yloxy)benzaldehyde (0.01 mol) was added dropwise, followed by sodium acetate (0.015 mol) to neutralize the hydrochloride salt. The reaction mixture was refluxed at 65 °C for 24 h under continuous stirring. After cooling to room temperature, the precipitated product was filtered, washed with cold methanol, and dried under vacuum.

HAG; Yield: 87%. Molecular formula:  $\text{C}_{18}\text{H}_{14}\text{N}_4\text{O}_2$ . M.W: 318.34 g/mol. m.p: 216°C. Color: Yellow. FT-IR ( $\text{cm}^{-1}$ ): 3328, 3173, 2102, 1609.  $^1\text{H}$  NMR (600 MHz, DMSO)  $\delta$  12.06 (s, 1H), 10.54 (s, 1H), 8.60 (s, 1H), 8.41 – 8.22 (m, 1H), 8.09 (s, 1H), 7.86 – 7.45 (m, 4H), 6.64 – 6.33 (m, 2H),

4.84 (d,  $J = 2.1$  Hz, 2H), 3.81 – 3.55 (m, 1H).  $^{13}\text{C}$  NMR (151 MHz, DMSO)  $\delta$  160.22, 159.13, 154.92, 146.88, 138.17, 132.61, 132.24, 132.01, 127.35, 126.88, 126.71, 124.09, 114.39, 107.40, 102.37, 79.53, 78.93, 56.02. Elemental analysis: Calcd. for  $\text{C}_{18}\text{H}_{14}\text{N}_4\text{O}_2$ : C, 67.92; H, 4.43; N, 17.60. Found: C, 67.78; H, 4.35; N, 17.51.

### 2.3 Synthesis of Ni(II), Zn(II) and Cu(II) Complexes

The Schiff base ligand was dissolved in 20 mL of ethanol, and a solution of the corresponding metal salt ( $\text{Ni}(\text{OAc})_2 \cdot 4\text{H}_2\text{O}$ ,  $\text{Zn}(\text{OAc})_2 \cdot 2\text{H}_2\text{O}$ , and  $\text{Cu}(\text{OAc})_2 \cdot \text{H}_2\text{O}$ ) dissolved in 20 mL of ethanol was added slowly under stirring. The resulting reaction mixture was refluxed under a condenser for 4 h. After completion of the reaction, the formed solid product was collected by filtration, washed with cold ethanol, and dried at room temperature.

$[\text{Ni}(\text{AG})_2]$ ; Yield: 85%. Molecular formula:  $\text{C}_{36}\text{H}_{26}\text{N}_8\text{O}_4\text{Ni}$ . M.W: 693.35 g/mol. Color: moss green. m.p.  $>280^\circ\text{C}$  decompose. FT-IR ( $\text{cm}^{-1}$ ): 3288, 2120, 1603, 590, 458. Elemental analysis: Calcd. for  $\text{C}_{36}\text{H}_{26}\text{N}_8\text{O}_4\text{Ni}$ : C, 62.36; H, 3.78; N, 16.16. Found: C, 62.26; H, 3.69; N, 16.23.

$[\text{Cu}(\text{AG})_2]$ ; Yield: 90%. Molecular formula:  $\text{C}_{36}\text{H}_{26}\text{N}_8\text{O}_4\text{Cu}$ . M.W: 698.20 g/mol. Color: brown. m.p.  $>280^\circ\text{C}$  decompose. FT-IR ( $\text{cm}^{-1}$ ): 3328, 3259, 3173, 2102, 1603, 567, 423. Elemental analysis: Calcd. for  $\text{C}_{36}\text{H}_{26}\text{N}_8\text{O}_4\text{Cu}$ : C, 61.93; H, 3.75; N, 16.05. Found: C, 61.85; H, 3.79; N, 16.01.

$[\text{Zn}(\text{AG})_2]$ ; Yield: 83%. Molecular formula:  $\text{C}_{36}\text{H}_{26}\text{N}_8\text{O}_4\text{Zn}$ . M.W: 700.04 g/mol. Color: yellow. m.p.  $>280^\circ\text{C}$  decompose. FT-IR ( $\text{cm}^{-1}$ ): 3330-3100, 2113, 1603, 590, 446. Elemental analysis: Calcd. for  $\text{C}_{36}\text{H}_{26}\text{N}_8\text{O}_4\text{Zn}$ : C, 61.77; H, 3.74; N, 16.01. Found: 61.64; H, 3.83; N, 15.89.

## 2.4 Minimum Inhibitory Concentration (MIC) Assay

The antimicrobial activity of the synthesized metal complexes was evaluated against three reference bacterial strains: *Escherichia coli* ATCC 35218, *Micrococcus luteus* ATCC 9341, and *Staphylococcus aureus* ATCC 25923. All strains were maintained on nutrient agar slants at 4 °C and subcultured on fresh agar plates 24 h before each experiment. Stock solutions of each compound were prepared in dimethyl sulfoxide (DMSO) and further diluted in Mueller–Hinton broth (MHB) to obtain the desired concentration range. Streptomycin (Str) was used as a reference antibiotic control and prepared in MHB at appropriate concentrations. MIC values were determined using the broth microdilution method in sterile flat-bottom 96-well microplates. Twofold serial dilutions of each compound were prepared in MHB to obtain a final concentration range that covered 31.25–2000 µg/mL in the wells. For the reference antibiotic streptomycin, a corresponding twofold serial dilution series was prepared in the same medium. All assays were performed in duplicate and the plates were incubated at 37 °C for 18 h under aerobic conditions. After incubation, bacterial viability was assessed using resazurin as a redox indicator. A resazurin solution was added to each well and the plates were further incubated at 37 °C for 4 h. The MIC was defined as the lowest concentration of the tested compound at which no visible color change was observed compared with the growth control [21].

## 2.5 Molecular Docking Simulations

The three-dimensional crystal structures of *Staphylococcus aureus* target proteins were retrieved from the Protein Data Bank (PDB). The following structures were used for docking analysis: Sortase A (PDB ID: 1T2W), DNA gyrase (PDB ID: 3U2D), FtsA (PDB ID: 3WQU), and undecaprenyl diphosphate synthase (UPPS; PDB ID: 4H8E). All co-crystallized ligands, water molecules, and heteroatoms were removed prior to docking to avoid interference with ligand binding. Missing residues were examined and, when necessary, corrected prior to energy optimization. Polar hydrogen atoms were added, and appropriate partial charges were assigned to the protein structures. The docking simulations were conducted using AutoDock Vina (version 1.1.2). The docking grid was defined to encompass the entire enzyme molecule, allowing unrestricted exploration of all possible binding sites. To assess the reliability of the predicted binding poses, the docking results were compared with the positions of the co-crystallized ligands in the corresponding crystal structures. The exhaustiveness parameter was set to 16 to balance computational time

and accuracy. The docking results were analyzed using Discovery Studio Visualizer to identify receptor–ligand interactions. Two-dimensional interaction diagrams were generated to illustrate the interaction profiles. In addition, the three-dimensional binding of the ligand on the protein surface was visualized using ChimeraX 1.9, allowing a better understanding of the spatial orientation and interaction topology.

## 3. Results and Discussion

In this work, a new hydralazine-based Schiff base ligand (HAG) was synthesized and characterized. The ligand was characterized by FTIR, <sup>1</sup>H/<sup>13</sup>C NMR and UV-Vis spectra. The ligand was reacted with Ni(II), Cu(II) and Zn(II) in 2:1 ratio (ligand:metal) to yield metal complexes with [M(AG)<sub>2</sub>]. The reaction scheme is given in Figure 1. The ligand and its metal complexes were obtained in high yield and compounds are stable in air.

The FTIR spectrum of the compounds were measured and characteristic bond stretching. FTIR measurements of the compounds were carried out on a Shimadzu IRTracer-100 using the ATR method. The spectra recorded in the 4000–450 cm<sup>-1</sup> range were evaluated by comparison with those of the free ligand to clarify the coordination behavior. The FTIR spectra of the HAG ligand and the [Zn(AG)<sub>2</sub>] complex, given as representative examples in Figures 2 and 3, are presented. The free ligand displays a characteristic band at 3328 cm<sup>-1</sup>, attributable to ν(O-H)/ν(N-H) stretching vibrations [2]. Weak signals observed at 2100–2120 cm<sup>-1</sup> in both the ligand and complexes correspond to ν(C≡C) of the alkyne moiety [22]. The disappearance of the ν(O-H) band upon complexation supports deprotonation of the phenolic group and its involvement in metal binding. In the Cu(II) and Zn(II) complexes, broad absorptions around 3330 and 3100 cm<sup>-1</sup> indicate ν(O-H) vibrations associated with coordinated or lattice water molecules [23]. Coordination through the phenolic oxygen is further evidenced by a 6–11 cm<sup>-1</sup> shift of the δ(O-H) in-plane bending band from its original position at 1483 cm<sup>-1</sup>. The ν(C=N) band of the free ligand was observed at 1609 cm<sup>-1</sup>, [23] consistent with literature values for hydrazone Schiff bases (1610–1645 cm<sup>-1</sup>). Upon complexation, this band shifted to 1603 cm<sup>-1</sup> (Δν ≈ 6 cm<sup>-1</sup>), indicating coordination through the azomethine nitrogen. Similar shifts (5–20 cm<sup>-1</sup>) have been reported for related hydralazine-derived complexes. Additionally, new absorption bands appearing in the 490–590 cm<sup>-1</sup> and 480–420 cm<sup>-1</sup> regions are assigned to ν(M-O) and ν(M-N) modes, confirming coordination through oxygen and nitrogen donor atoms.

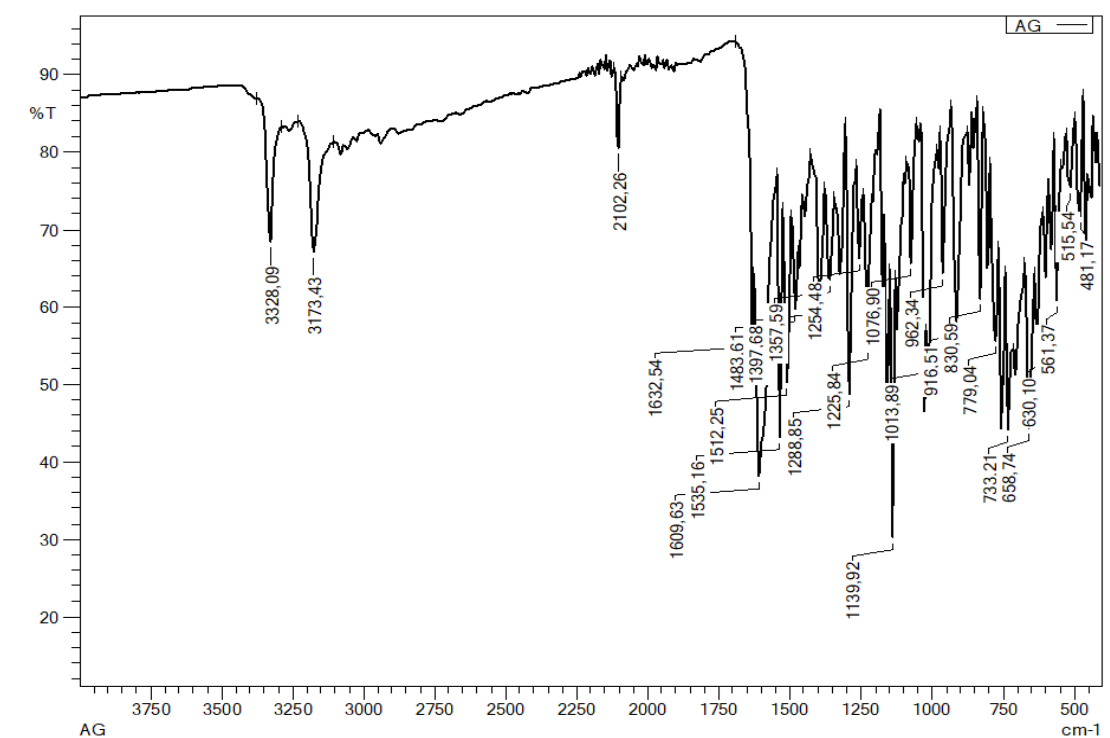
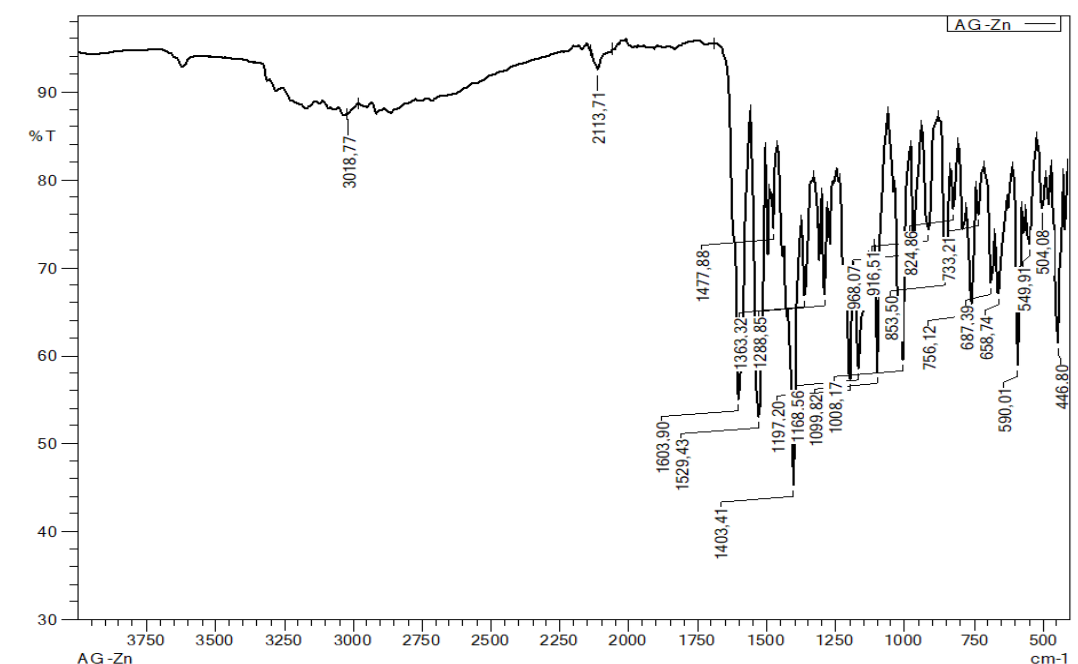


Figure 2. FT-IR spectrum of the ligand HAG.

Figure 3. FT-IR spectrum of Zn(II) complex  $[Zn(AG)_2]$ .

The  $^1H$  and  $^{13}C$  NMR spectra of the ligand (HAG) were measured in  $d_6$ -DMSO. The  $^1H$  and  $^{13}C$  NMR spectra are shown in Figs. 4 and 5. In the  $^1H$  spectrum of the ligand, the singlet peaks at 12.06 (s,  $^1H$ ) and 10.54 (s,  $^1H$ ) ppm are assigned to the -OH and -NH protons, respectively. The imine proton (N=CH) resonates at 8.60 ppm. The aromatic protons were observed as multiplet peaks at 8.41-6.33 ppm range. The singlet peaks at 4.84 and 3.55 ppm are

due to the proton of  $OCH_2-$  and  $C\equiv C-H$  groups, respectively. The signal integration values are compatible with expected structure. In the  $^{13}C$  spectrum of the ligand, the peak 160.22 ppm is due to carbon signal of azomethine group. The aromatic peaks are seen at 159.13 and 102.37 ppm range. The aliphatic carbon atom signals ( $OCH_2-C\equiv CH$ ) were seen at 79.53, 78.93 and 56.02 ppm.

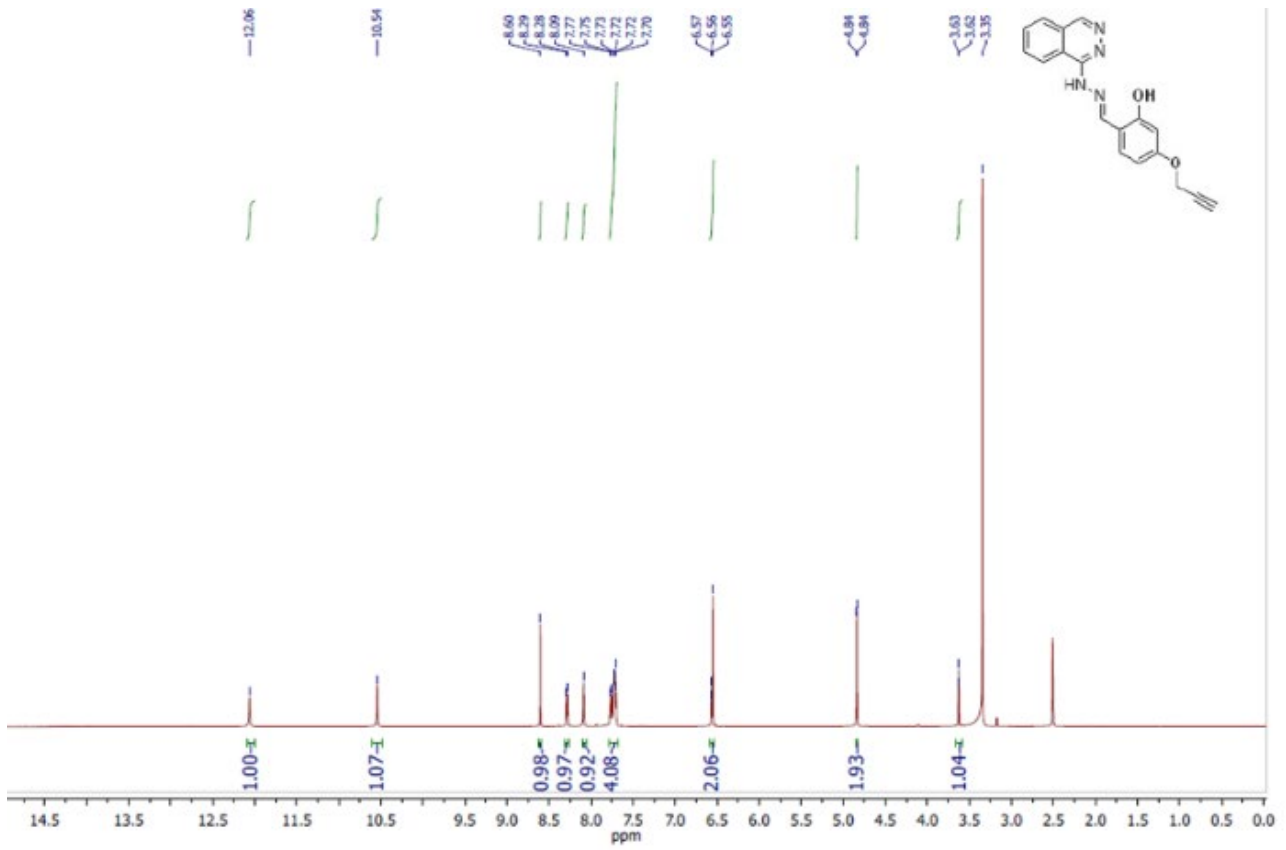


Figure 4. <sup>1</sup>H NMR Spectrum of HAG.

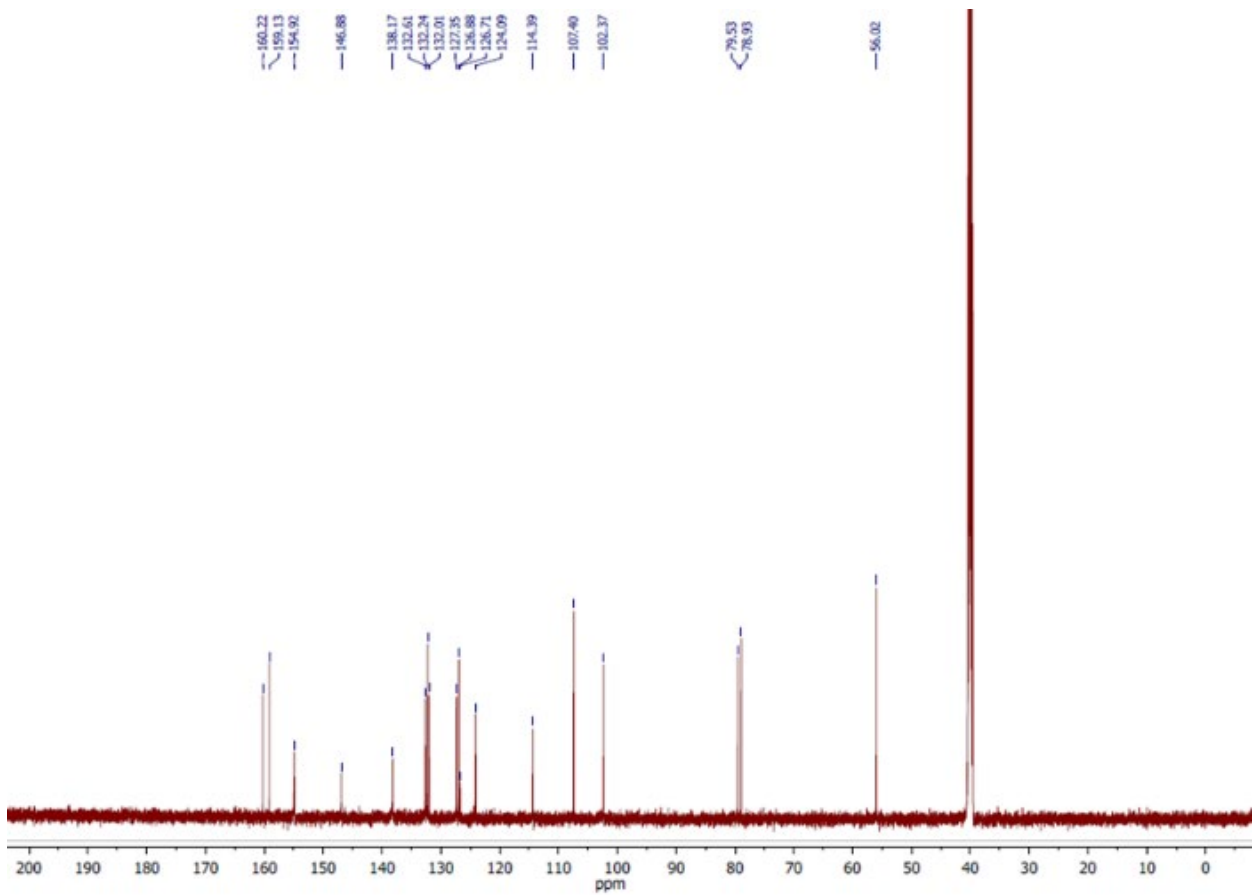


Figure 5. <sup>13</sup>C NMR Spectrum of HAG.

The UV-vis spectra of the ligand and its metal complexes were studied in DMF ( $10^{-5}$  M). In the UV-Vis spectra, the ligand exhibited a  $\pi \rightarrow \pi^*$  transition at 382 nm, while the metal complexes showed bathochromic shifts (392–467 nm), attributed to ligand-to-metal charge transfer (LMCT) transitions (Figure 6). Comparable red shifts have been reported for Cu(II) and Zn(II) hydrazone complexes in the 400–500 nm region. In the spectra of Zn(II) complex, there are four absorption bands at

maximum 392, 416, 440 and 467 nm. The absorption bands can be assigned to the  $\pi\text{-}\pi^*$  electronic transitions and charge transition band. The  $\pi\text{-}\pi^*$  electronic transition of the ligand are red-shifted in the spectrum of all complexes. In spectra of Ni(II) complex, the absorption bands of  $\pi\text{-}\pi^*$  transitions are seen at 383, 396 and 421 nm. The relatively weak band at 453 nm is attributed to charge transition. The Cu(II) complex showed three absorption maxima at 395, 430 and 456 nm.

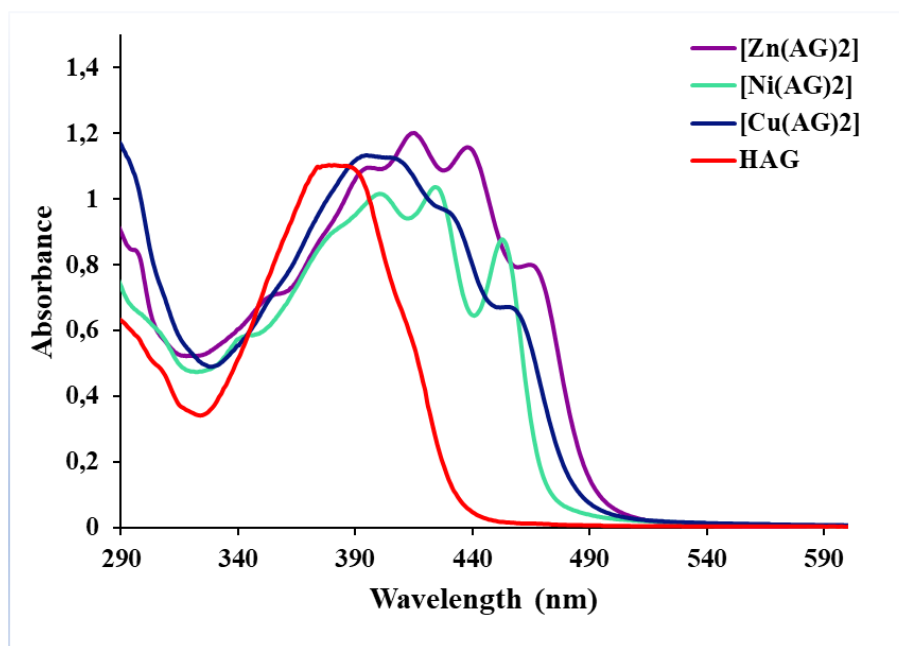


Figure 6. UV-Vis spectra of the compounds in DMF ( $1.0 \times 10^{-5}$  M).

### 3.1 The Antimicrobial Activities

The antimicrobial activities of  $[\text{Cu}(\text{AG})_2]$ ,  $[\text{Ni}(\text{AG})_2]$  and  $[\text{Zn}(\text{AG})_2]$  complexes were evaluated against *Escherichia coli* ATCC 35218, *Micrococcus luteus* ATCC 9341, and *Staphylococcus aureus* ATCC 25923 using the minimum inhibitory concentration (MIC) method. The results clearly demonstrated that the antimicrobial efficacy varied depending on both the microbial strain and the metal ion coordinated to the ligand (Table 1). Among the tested compounds,  $[\text{Zn}(\text{AG})_2]$  exhibited the strongest antimicrobial activity against *Staphylococcus aureus*, with a MIC value of 250  $\mu\text{g}/\text{mL}$ , indicating a notably higher potency compared to  $[\text{Cu}(\text{AG})_2]$  and  $[\text{Ni}(\text{AG})_2]$ , both of which showed MIC values of 1000  $\mu\text{g}/\text{mL}$  against the same strain. This finding demonstrates that zinc coordination significantly enhanced antibacterial activity against *S. aureus*. Additionally,  $[\text{Zn}(\text{AG})_2]$  also showed moderate efficacy against *Micrococcus luteus* (MIC = 500  $\mu\text{g}/\text{mL}$ ),  $[\text{Cu}(\text{AG})_2]$  whereas and  $[\text{Ni}(\text{AG})_2]$  exhibited weaker effects, requiring higher concentrations for inhibition (1000 and 2000  $\mu\text{g}/\text{mL}$ , respectively). In contrast,  $[\text{Cu}(\text{AG})_2]$  and  $[\text{Ni}(\text{AG})_2]$  displayed weaker antimicrobial activity against *M. luteus* and *S. aureus* than against *E. coli*, indicating lower efficacy of Cu(II) and Ni(II) complexes toward the tested Gram-positive bacteria. The standard antibiotic streptomycin exhibited markedly stronger

activity against all bacterial strains, with MIC values of 25–50  $\mu\text{g}/\text{mL}$ . The enhanced activity of Zn(II) complexes has been reported in several studies. Bakale et al. (2018) demonstrated that Zn(II) and Cu(II) complexes of hydrazone derivatives exhibited superior biological activity compared to the free ligand, particularly against Gram-positive strains [24]. Similarly, Althobiti and Zabin (2020) reported that Zn(II) complexes of Schiff base ligands displayed pronounced inhibition zones against *S. aureus* and *E. faecalis*, while showing reduced activity against Gram-negative bacteria [25]. Patil et al. (2023) also reported that the antibacterial efficiency of metal complexes strongly depends on both the metal center and ligand framework, with certain Zn and Ni complexes demonstrating enhanced activity against *S. aureus* compared to other strains [26].

Table 1. Antimicrobial activities of compounds (MIC,  $\mu\text{g}/\text{mL}$ )

	$[\text{Cu}(\text{AG})_2]$	$[\text{Ni}(\text{AG})_2]$	$[\text{Zn}(\text{AG})_2]$	Str
<i>Escherichia coli</i> ATCC 35218	500	500	500	50
<i>Micrococcus luteus</i> ATCC 9341	1000	2000	500	25
<i>Staphylococcus aureus</i> ATCC 25923	1000	1000	250	25

### 3.2 Molecular Docking Simulations

Based on the minimum inhibitory concentration (MIC) results,  $[Zn(AG)_2]$  exhibited the highest antibacterial activity against *Staphylococcus aureus* compared with the other tested complexes. Therefore, molecular docking

analysis was specifically focused on *S. aureus* target proteins, and  $[Zn(AG)_2]$  was selected as the ligand for all docking experiments in order to explore the possible molecular basis of its antibacterial activity.

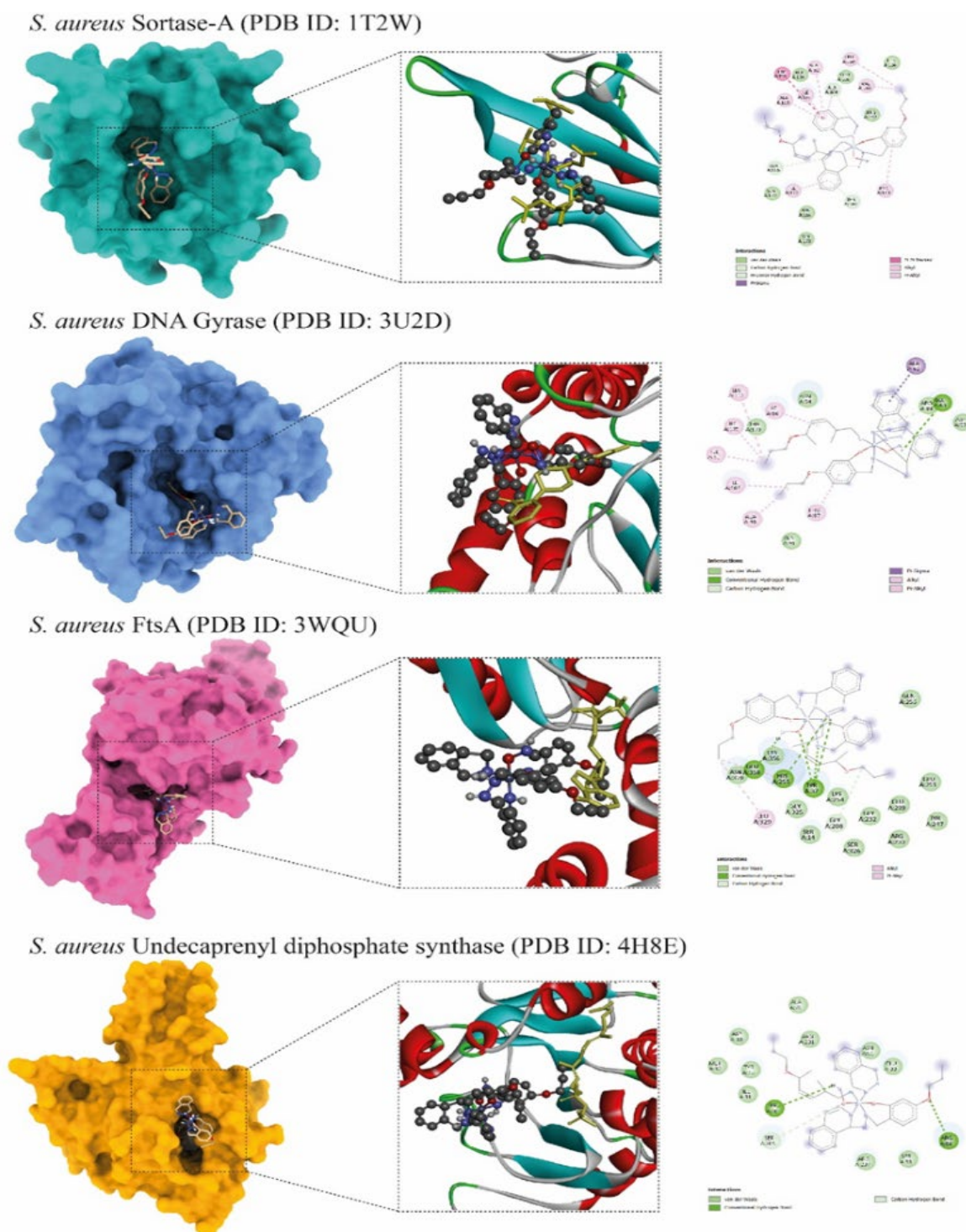


Figure 7. Surface representation and active-site docking poses of  $[Zn(AG)_2]$  within (A) Sortase A, (B) FtsA, (C) DNA gyrase, and (D) undecaprenyl diphosphate synthase (UPPS). Insets show detailed views of  $[Zn(AG)_2]$  interactions within the active pockets. Right panels illustrate two-dimensional ligand interaction diagrams highlighting hydrogen bonding and hydrophobic contacts between  $[Zn(AG)_2]$  and active site residues.  $[Zn(AG)_2]$  is shown in ball and stick representation, while the co-crystallized ligands are displayed in stick representation and colored in yellow. Co-crystallized ligands are LEU-PRO-GLU-THR-GLY (Sortase A), an ATP-competitive inhibitor (DNA gyrase), ATP (FtsA), and farnesyl diphosphate (UPPS), respectively.

Molecular docking analysis was performed to evaluate the interaction of [Zn(AG)<sub>2</sub>] with four essential *Staphylococcus aureus* proteins with available crystal structures complexed with known ligands: Sortase A (PDB ID: 1T2W), DNA gyrase (PDB ID: 3U2D), FtsA (PDB ID: 3WQU), and undecaprenyl diphosphate synthase (UPPS; PDB ID: 4H8E). In all docking analysis, [Zn(AG)<sub>2</sub>] displayed favorable binding energies, indicating stable ligand–protein interactions. For Sortase A, which is crystallized with the pentapeptide LEU–PRO–GLU–THR–GLY occupying the catalytic pocket, [Zn(AG)<sub>2</sub>] demonstrated a strong binding affinity of –8.5 kcal/mol. Importantly, structural alignment showed that [Zn(AG)<sub>2</sub>] was positioned within the same catalytic groove as the co-crystallized peptide, suggesting possible competition with the natural substrate motif and potential effect of the transpeptidation protein.

In the case of DNA gyrase, whose structure contains the inhibitor 4-bromo-5-methyl-N-[1-(3-nitropyridin-2-yl)piperidin-4-yl]-1H-pyrrole-2-carboxamide bound to the ATP-binding domain of GyrB, [Zn(AG)<sub>2</sub>] showed the highest binding energy among all tested targets (–8.7 kcal/mol). Docking results indicated that [Zn(AG)<sub>2</sub>] occupied the same ATP-binding pocket as the co-crystallized compound, supporting the possibility that [Zn(AG)<sub>2</sub>] may interact with residues in ATP binding. For FtsA, whose crystal structure includes adenosine 5'-triphosphate (ATP) bound to the nucleotide-binding site, [Zn(AG)<sub>2</sub>] yielded a binding energy of –7.7 kcal/mol. Docking analysis revealed that [Zn(AG)<sub>2</sub>] localized at the ATP-binding cleft, suggesting a potential interaction within this functional region.

UPPS was crystallized in complex with farnesyl diphosphate, a substrate intermediate in isoprenoid biosynthesis. [Zn(AG)<sub>2</sub>] exhibited a binding energy of –8.1 kcal/mol and localized within the same cavity that accommodates farnesyl diphosphate. This co-localization suggests that [Zn(AG)<sub>2</sub>] may interact with the substrate-binding region. Collectively, docking analysis demonstrated that [Zn(AG)<sub>2</sub>] consistently occupied the functional binding sites across all four proteins. While these findings provide insight into possible molecular interactions, they should be interpreted as theoretical predictions that require experimental confirmation.

#### 4. Conclusions

In this study, a new hydralazine-based Schiff base ligand (HAG) and its Ni(II), Cu(II), and Zn(II) complexes were successfully synthesized and fully characterized using elemental analysis and spectroscopic techniques. Spectral data confirmed that the ligand coordinates to the metal ions in a tridentate fashion through phenolate oxygen, azomethine nitrogen, and phthalazine nitrogen atoms, resulting in stable [M(AG)<sub>2</sub>] complexes. The antibacterial evaluation revealed that metal coordination plays a crucial role in enhancing biological activity. Among the investigated complexes, the Zn(II) complex exhibited the strongest Antibacterial Activity, particularly against

*Staphylococcus aureus*. Molecular docking studies supported the experimental findings by demonstrating favorable binding of [Zn(AG)<sub>2</sub>] to essential *S. aureus* enzymes involved in cell wall biosynthesis, DNA replication, and cell division.

#### Conflict of Interest

There are no conflicts of interest in this work.

#### References

- [1] Sousa, C., Freire, C., & De Castro, B. (2003). Synthesis and characterization of benzo-15-crown-5 ethers with appended N<sub>2</sub>O Schiff bases. *Molecules*, 8(12), 894-900. <https://doi.org/10.3390/81200894>
- [2] El-Sherif, A. A., Shoukry, M. M., & Abd-Elgawad, M. M. (2012). Synthesis, characterization, biological activity and equilibrium studies of metal (II) ion complexes with tridentate hydrazone ligand derived from hydralazine. *Spectrochimica Acta Part A: Molecular and Biomolecular Spectroscopy*, 98, 307-321. <http://dx.doi.org/10.1016/j.saa.2012.08.034>
- [3] Soliman, S. M., Massoud, R. A., Al-Rasheed, H. H., & El-Faham, A. (2021). Molecular and supramolecular structures of Cd (II) complexes with hydralazine-based ligands; a new example for cyclization of hydrazonephthalazine to triazolophthalazine. *Crystals*, 11(7), 823. <https://doi.org/10.3390/cryst11070823>
- [4] Liu, D. C., Gong, G. H., Wei, C. X., Jin, X. J., & Quan, Z. S. (2016). Synthesis and anti-inflammatory activity evaluation of a novel series of 6-phenoxy-[1, 2, 4] triazolo [3, 4-a] phthalazine-3-carboxamide derivatives. *Bioorganic & Medicinal Chemistry Letters*, 26(6), 1576-1579. <https://doi.org/10.1016/j.bmcl.2016.02.008>
- [5] Soliman, S. M., Albering, J. H., Farooq, M., Wadaan, M. A., & El-Faham, A. (2017). Synthesis, structural and biological studies of two new Co (III) complexes with tridentate hydrazone ligand derived from the antihypertensive drug hydralazine. *Inorganica Chimica Acta*, 466, 16-29. <https://doi.org/10.1016/j.ica.2017.05.045>
- [6] Holló, B., Magyari, J., Živković-Radovanović, V., Vučković, G., Tomić, Z. D., Szilágyi, I. M., ... & Szécsényi, K. M. (2014). Synthesis, characterisation and antimicrobial activity of bis (phthalazine-1-hydrazone)-2, 6-diacetylpyridine and its complexes with Co(II), Ni(II), Cu(II) and Zn(II). *Polyhedron*, 80, 142-150. <https://doi.org/10.1016/j.poly.2014.03.007>
- [7] Issac, Y., El-Karim, E., Donia, S., & Behalaw, M. (2002). Novel synthesis of phthalazine derivatives as antimicrobial agents. *Sulfur Letters*, 25(4), 183-190. <https://doi.org/10.1080/02786110213977>
- [8] El-Hashash, M. A. A., Soliman, A. Y., & ELSHAMY, I. E. (2012). Synthesis and antimicrobial evaluation of some annelated phthalazine derivatives and acyclo C-nucleosides from 1-chloro-4-(2, 4, 6-trimethylphenyl) phthalazine precursor. *Turkish Journal of Chemistry*, 36(3), 347-366. <https://doi.org/10.3906/kim-1111-52>
- [9] Nuha, D., Evren, A. E., Özkan, B. N. S., Gundogdu-Karaburun, N., & Karaburun, A. Ç. (2024). Design, synthesis, biological evaluation, and molecular modeling simulations of new phthalazine-1, 4-dione derivatives as anti-Alzheimer's agents. *Archiv der Pharmazie*, 357(10), e2400067. <https://doi.org/10.1002/ardp.202400067>

- [10] Amin, K. M., Barsoum, F. F., Awadallah, F. M., & Mohamed, N. E. (2016). Identification of new potent phthalazine derivatives with VEGFR-2 and EGFR kinase inhibitory activity. *European Journal of Medicinal Chemistry*, *123*, 191-201. <https://doi.org/10.1016/j.ejmech.2016.07.049>
- [11] Wasfy, A. F., Aly, A. A., Behalo, M. S., & Mohamed, N. S. (2013). An efficient synthesis of some new 1, 4-disubstituted phthalazine derivatives and their anticancer activity. *Der PharmaChemica*, *5*, 82-96.
- [12] Kogan, V. A., Levchenkov, S. I., Popov, L. D., & Shcherbakov, I. A. (2009). 1-Hydrazinophthalazine based hydrazones and their transition metal complexes: Structure and biological activity. *Russian Journal of General Chemistry*, *79*(12), 2767-2775. <https://doi.org/10.1134/S1070363209120354>
- [13] Kadhim, U. A., & Abbas, A. F. (2024). Synthesis, Characterization and Microbiological Activities of a new Schiff Base Derived from Hydralazine Hydrochloride. *Basrah Journal of Science*, *42*(2), 307-320.
- [14] Gatto, C. C., Dias, L. M., Paiva, C. A., da Silva, I. C., Freire, D. O., Tormena, R. P., ... & Martins, J. B. (2024). Effects of changing ions on the crystal design, non-covalent interactions, antimicrobial activity, and molecular docking of Cu (II) complexes with a pyridoxal-hydrazone ligand. *Frontiers in Chemistry*, *12*, 1347370. <https://doi.org/10.3389/fchem.2024.1347370>
- [15] Khalil, T. E., Soliman, S. M., Khalil, N. A., El-Faham, A., Foro, S., & El-Dissouky, A. (2022). Synthesis, structure, X-ray photoelectron spectroscopy (XPS), and antimicrobial, anticancer, and antioxidant activities of Co (III) complexes based on the antihypertensive hydralazine. *Applied Organometallic Chemistry*, *36*(3), e6565. <https://doi.org/10.1002/aoc.6565>
- [16] Molodykh, Z. V., Lisenkova, A. N., Buzykin, B. I., & Kitaev, Y. P. (1977). Anthelmintic activity of some hydrazones. *Pharmaceutical Chemistry Journal*, *11*(1), 74-76.
- [17] Khalil, T. E., Dahlous, K. A., Soliman, S. M., Khalil, N. A., El-Faham, A., & El-Dissouky, A. (2022). Synthesis, X-ray structure and biological studies of new self-assembled Cu (II) complexes derived from s-triazine Schiff base ligand. *Molecules*, *27*(9), 2989. <https://doi.org/10.3390/molecules27092989>
- [18] He, H., Wang, X., Shi, L., Yin, W., Yang, Z., He, H., & Liang, Y. (2016). Synthesis, antitumor activity and mechanism of action of novel 1, 3-thiazole derivatives containing hydrazide-hydrazone and carboxamide moiety. *Bioorganic & medicinal chemistry letters*, *26*(14), 3263-3270. <https://doi.org/10.1016/j.bmcl.2016.05.059>
- [19] Selvarani, V., Annaraj, B., Neelakantan, M. A., Sundaramoorthy, S., & Velmurugan, D. (2013). Synthesis, characterization and crystal structures of copper (II) and nickel (II) complexes of propargyl arm containing N2O2 ligands: antimicrobial activity and DNA binding. *Polyhedron*, *54*, 74-83. <https://doi.org/10.1016/j.poly.2013.02.030>
- [20] Güngör, S. A., Tümer, M., Köse, M., & Erkan, S. (2020). Benzaldehyde derivatives with functional propargyl groups as  $\alpha$ -glucosidase inhibitors. *Journal of Molecular Structure*, *1206*, 127780. <https://doi.org/10.1016/j.molstruc.2020.127780>
- [21] Avşar, C., Findik, B. T., Dede, B., Erdem-Tuncmen, M., & Karipcin, F. (2025). Transition metal complexes of N-furfuryl-N'-benzoylthiourea: A study of synthesis, antibacterial activities, quantum chemical calculations and molecular modeling simulations. *Polyhedron*, *267*, 117357. <https://doi.org/10.1016/j.poly.2024.117357>
- [22] Dağ, A. K., Köse, A., Tüzün, G., & Sayın, K. (2025). A Schiff base and triazolophthalazine derivatives of hydralazine: Crystal structures, DNA binding properties and DFT studies. *Journal of Molecular Structure*, *144532*. <https://doi.org/10.1016/j.molstruc.2025.144532>
- [23] Bakale, R. P., Naik, G. N., Machakanur, S. S., Mangannavar, C. V., Muchchandi, I. S., & Gudasi, K. B. (2018). Structural characterization and antimicrobial activities of transition metal complexes of a hydrazone ligand. *Journal of Molecular Structure*, *1154*, 92-99. <https://doi.org/10.1016/j.molstruc.2017.10.035>
- [24] Althobiti, H. A., & Zabin, S. A. (2020). New Schiff bases of 2-(quinolin-8-yloxy) acetohydrazide and their Cu (II), and Zn (II) metal complexes: their in vitro antimicrobial potentials and in silico physicochemical and pharmacokinetics properties. *Open Chemistry*, *18*(1), 591-607. <https://doi.org/10.1515/chem-2020-0085>
- [25] Patil, S. S., Tadavi, S. K., Ghatole, A. M., & Bendre, R. S. (2023). Transition metal complexes of pyridazine-based ligand: synthesis, characterization, biological activities, and molecular docking studies. *Journal of the Iranian Chemical Society*, *20*(12), 3103-3117. <https://doi.org/10.1007/s13738-023-02901-y>